frontiers in Earth Science

ORIGINAL RESEARCH
published: 29 July 2021
doi: 10.3389/feart.2021.661311

One Year of Seismicity Recorded Through Ocean Bottom Seismometers Illuminates Active Tectonic Structures in the Ionian Sea (Central Mediterranean)

Tiziana Sgroi[1], Alina Polonia[2], Laura Beranzoli[1], Andrea Billi[3], Alessandro Bosman[3], Antonio Costanza[4], Marco Cuffaro[3], Giuseppe D'Anna[4], Mariagrazia De Caro[1], Maria Di Nezza[1], Gioacchino Fertitta[4], Francesco Frugoni[1], Luca Gasperini[2], Stephen Monna[1], Caterina Montuori[1], Lorenzo Petracchini[3], Patrizio Petricca[5], Stefania Pinzi[6], Andrea Ursino[4] and Carlo Doglioni[5,7]*

[1]Istituto Nazionale di Geofisica e Vulcanologia, Sezione Roma 2, Roma, Italy, [2]Istituto di Scienze Marine, CNR, Bologna, Italy, [3]Istituto di Geologia Ambientale e Geoingegneria, CNR, Roma, Italy, [4]Istituto Nazionale di Geofisica e Vulcanologia, Osservatorio Etneo, Sezione di Catania, Catania, Italy, [5]Dipartimento di Scienze della Terra, Sapienza Università di Roma, Roma, Italy, [6]Istituto Nazionale di Geofisica e Vulcanologia, Sezione Roma 1, Roma, Italy, [7]Istituto Nazionale di Geofisica e Vulcanologia, Roma, Italy

OPEN ACCESS

Edited by:
Susan Bilek,
New Mexico Institute of Mining and Technology, United States

Reviewed by:
Piero Poli,
Université Grenoble Alpes, France
Francisco Javier Nuñez-Cornu,
University of Guadalajara, Mexico

***Correspondence:**
Andrea Billi
andrea.billi@cnr.it

Specialty section:
This article was submitted to Solid Earth Geophysics, a section of the journal Frontiers in Earth Science

Received: *30 January 2021*
Accepted: *14 July 2021*
Published: *29 July 2021*

Citation:
Sgroi T, Polonia A, Beranzoli L, Billi A, Bosman A, Costanza A, Cuffaro M, D'Anna G, De Caro M, Di Nezza M, Fertitta G, Frugoni F, Gasperini L, Monna S, Montuori C, Petracchini L, Petricca P, Pinzi S, Ursino A and Doglioni C (2021) One Year of Seismicity Recorded Through Ocean Bottom Seismometers Illuminates Active Tectonic Structures in the Ionian Sea (Central Mediterranean). Front. Earth Sci. 9:661311. doi: 10.3389/feart.2021.661311

Seismological data recorded in the Ionian Sea by a network of seven Ocean Bottom Seismometers (OBSs) during the 2017–2018 SEISMOFAULTS experiment provides a close-up view of seismogenic structures that are potential sources of medium-high magnitude earthquakes. The high-quality signal-to-noise ratio waveforms are observed for earthquakes at different scales: teleseismic, regional, and local earthquakes as well as single station earthquakes and small crack events. In this work, we focus on two different types of recording: 1) local earthquakes and 2) Short Duration Events (SDE) associated to micro-fracturing processes. During the SEISMOFAULTS experiment, 133 local earthquakes were recorded by both OBSs and land stations (local magnitude ranging between 0.9 and 3.8), while a group of local earthquakes (76), due to their low magnitude, were recorded only by the OBS network. We relocated 133 earthquakes by integrating onshore and offshore travel times and obtaining a significant improvement in accuracy, particularly for the offshore events. Moreover, the higher signal-to-noise ratio of the OBS network revealed a significant seismicity not detected onshore, which shed new light on the location and kinematics of seismogenic structures in the Calabrian Arc accretionary prism and associated to the subduction of the Ionian lithosphere beneath the Apennines. Other signals recorded only by the OBS network include a high number of Short Duration Events (SDE). The different waveforms of SDEs at two groups of OBSs and the close correlation between the occurrence of events recorded at single stations and SDEs suggest an endogenous fluid venting from mud volcanoes and active fault traces. Results from the analysis of seismological data collected during the SEISMOFAULTS experiment confirm the necessity and potential of marine studies with OBSs, particularly in those geologically active areas of the Mediterranean Sea prone to high seismic risk.

Keywords: ocean bottom seismometer (OBS), local earthquakes, short duration events (SDE), Ionian Sea (Italy), Calabrian Arc, marine network, SEISMOFAULTS, active faults

INTRODUCTION

The lithosphere beneath the Ionian Sea is an oceanic embayment (Catalano et al., 2001), which is subducting contemporaneously beneath the Apennines and the Hellenides (Carminati et al., 2012; Carminati et al., 2020). The related accretionary prisms form two major salients within the depressed basin. The Ionian basin and its margins are among the most seismically active areas in the Mediterranean region. Here, some of the strongest earthquakes took place during historical and recent times, including the largest events ever recorded in Italy (e.g., 1169, Mw 6.6; 1693, Mw 7.4; 1908, Mw 7.2; 1990, Mw 5.7; Boschi et al., 1997). Despite many studies and large sets of data collected during marine geological campaigns (Bianca et al., 1999; Argnani and Bonazzi, 2005; Polonia et al., 2011; Gutscher et al., 2016), the offshore location of seismogenic sources and causative faults of large magnitude historical earthquakes are still debated. Part of the problem is the inadequacy of the onshore seismic network in locating medium-low-magnitude earthquakes occurring offshore. In fact, the location of these events based solely on land station recordings appears affected by considerable errors (Sgroi et al., 2006; Sgroi et al., 2021).

For the offshore records, land seismic observations suffer particularly from insufficient azimuthal coverage, which results in misdetection (or non-detection) of small-to-moderate magnitude earthquakes. These limits can be overcome by implementing networks of Ocean Bottom Seismometers (OBSs), designed as self-contained data acquisition systems deployed at the seafloor, where they are able to self-install and record ground motion data with high signal-to-noise ratio. The OBSs constitute the bulk modules or multi-sensor seafloor observatories, a new class of instruments, which are changing our knowledge of geologic processes in seas and oceans, gathering useful data for a variety of scientific investigations ranging from the deep Earth's structure to surface processes (e.g., Favali and Beranzoli, 2006; Billi et al., 2020).

Since the '80s, thanks to the technological development, OBSs and seafloor observatories have been deployed in different regions of the world, mainly to improve location of earthquakes occurring offshore and in coastal areas, complementing data from land based networks (e.g., Lawton et al., 1982; Hino et al., 1996; Hsiao et al., 2014), and to perform 1D and 3D seismic velocity crustal studies in the offshore (e.g., Husen et al., 2000; Montuori et al., 2007; Chang et al., 2008; Monna et al., 2013; Sgroi et al., 2021).

In recent years, several seismological experiments have been carried out in the Tyrrhenian and Ionian seas, with the deployment of OBSs and seafloor observatories (Dahm et al., 2002; Favali et al., 2015; Coltelli et al., 2016). In the southern Tyrrhenian Sea, an OBS network surrounding the Aeolian Islands operated for six months during the TYDE experiment (Dahm et al., 2002), detecting an intense seismicity of tectonic and volcanic origins (Sgroi et al., 2006; Sgroi et al., 2009). In the Ionian Sea, the deployment of the NEMO-SN1 seafloor observatory (Favali and Beranzoli, 2006) allowed for synchronous recordings of time-series for multidisciplinary studies and provided useful information on oceanic areas and, in particular, on volcanic and tectonic structures (Sgroi et al., 2007; Sgroi et al., 2014; Sgroi et al., 2019; Sgroi et al., 2021).

The SEISMOFAULTS project (www.seismofaults.it) has been the first experiment designed to illuminate geological active features offshore Sicily and south Calabria through the deployment of an OBS network (Billi et al., 2020). The SEISMOFAULTS main purpose was to explore seismicity of the submerged portion of the Calabrian Arc subduction complex, starting from observations carried out during marine geophysical/geological expeditions in the Ionian Sea (Polonia et al., 2016).

To gather information on the location of active tectonic features, we analysed data from a broad-band array of seven OBSs deployed in the Ionian Sea from May 2017 to May 2018, which recorded several thousands of distinct events including teleseismic, regional, and local earthquakes. Below, the character of seismic events is defined in terms of their spatial and temporal distribution, and in relation with the knowledge of the present tectonic setting (**Figure 1**). We acknowledge that the OBS network has significantly improved the determination of seismic events in the offshore and along the coasts. It has also allowed investigating the nature of seismogenic structures in the Ionian Sea through analysis of the microseismicity consisting of several thousands of low-magnitude earthquakes and short duration events (SDE), the latter suggesting microfracturing processes, endogenous venting from presumably active faults, and active geofluid venting from mud volcanoes.

TECTONIC SETTING

The Ionian Sea is located within the deformed Africa-Eurasia plate boundary in the Mediterranean region, where slab retreat occurs along the Calabrian Arc subduction (Doglioni, 1991; Devoti et al., 2008), i.e., the subduction hinge diverges relative to the upper Eurasian plate (**Figure 1**). The Calabrian Arc evolved on top of a NW-dipping subduction system where the subducting Ionian lithosphere sinks into the mantle forming subduction zone with a wide accretionary complex in the Calabrian Arc (Doglioni et al., 1999; Polonia et al., 2011; Maesano et al., 2017) and intense back-arc volcanism along the Aeolian Arc in Tyrrhenian Sea (Peccerillo, 2005). Present-day plate motion occurs in this region at slow velocities, in the order of a few mm/yr, as determined by space geodesy measurements (Devoti et al., 2008; Palano et al., 2015), accommodating mostly shortening inside the accretionary wedge and along the outer deformation front of the subduction arc (Doglioni et al., 1999; Polonia et al., 2011; Gallais et al., 2012, and references therein). In the Ionian Sea, the Calabrian accretionary prism is bounded towards the SW by the Malta Escarpment (**Figure 1**), where the Ionian salient along its western

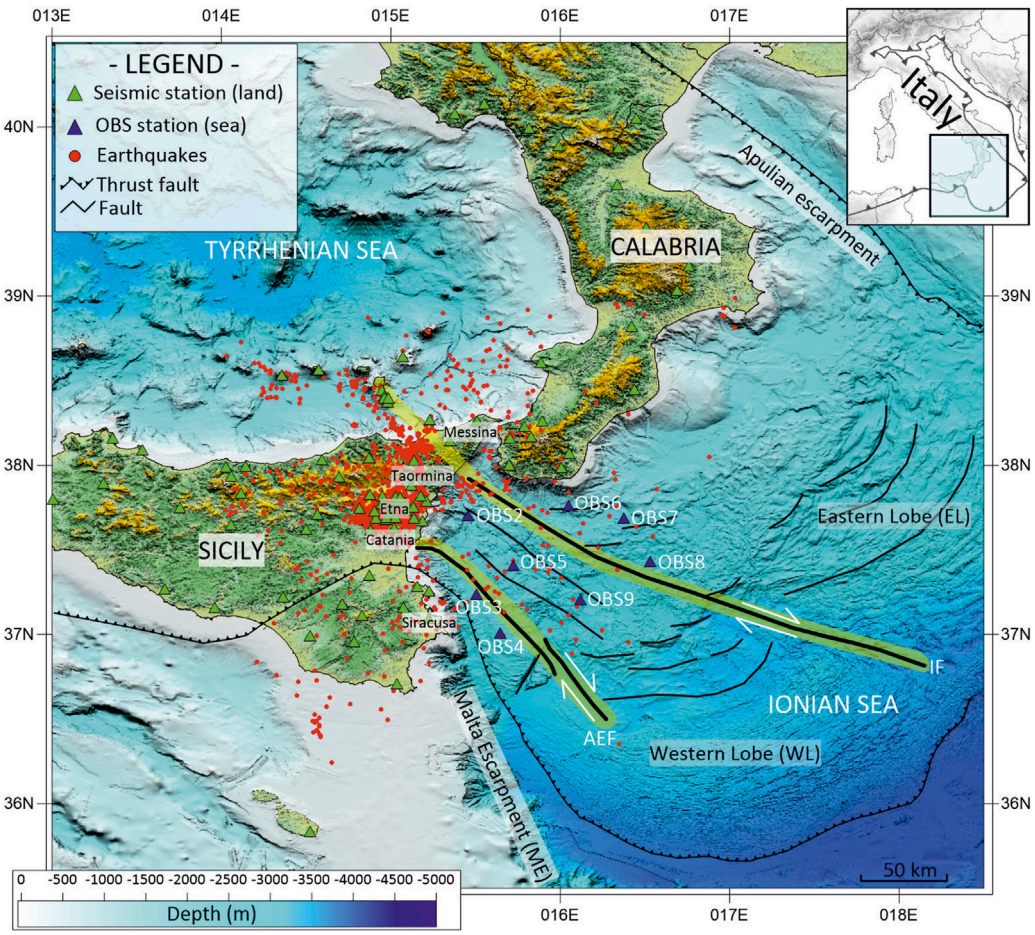

FIGURE 1 | Morphological map of the Western Ionian Sea and surroundings, indicating: main geological features, including Alfeo-Etna Fault (AEF) and Ionian Fault (IF) systems (Polonia et al., 2016), and Malta escarpment (ME); seismic stations used in this work (filled green triangles are land stations; filled blue triangles represent the OBSs); red dots indicate the locations of earthquakes from the land seismic bulletin of INGV and occurring during the SEISMOFAULTS experiment. About 2,400 events were located by INGV seismological network. Bathymetric data were obtained from high resolution multibeam soundings during the SEISMOFAULTS first cruise (Cuffaro et al., 2019; Billi et al., 2020) and merged with DEMs from https://portal.emodnet-bathymetry.eu/.

right-lateral transpressive segment merges into the Hyblean recess inland Sicily, cross-cutting the underlying Malta escarpment (Mariotti and Doglioni, 2000; Doglioni et al., 2001).

The Calabrian wedge in the Ionian Sea is characterized by sectors with different rheology and tectonic architectures: 1) the post-Messinian accretionary wedge; 2) the pre-Messinian accretionary wedge; and 3) the inner plateau, as described by Polonia et al. (2011). Generally, the post-Messinian and the pre-Messinian accretionary wedges include thick layers of evaporites and Tertiary/Mesozoic sediments, respectively. Fault zones are detected in the area between the pre-Messinian accretionary prism and the flat inner plateau, with a diffuse presence of mud volcanism (Loher et al., 2018; Cuffaro et al., 2019, and references therein).

Long fault lineaments and NW-SE transverse deformation zones cut through the NE-SW-trending Calabrian accretionary prism (**Figure 1**). Most of such structures are active and characterized by right-lateral to transtensional kinematics (Polonia et al., 2011, 2016, 2017a; Gallais et al., 2012, Gallais et al., 2013; Gutscher et al., 2016; Bortoluzzi et al., 2017). Some of them represent the surface expression of deep geodynamic processes, as suggested by mantle diapirs detected along the faults (Polonia et al., 2017).

Two major fault systems with opposite dip are identified in the region, i.e., the Ionian Fault (IF) and the Alfeo-Etna Fault (AEF) systems (**Figure 1**). The IF separates two distinct sectors of the Calabrian accretionary prism, the western and the eastern lobes (WL, offshore Sicily; EL, offshore Calabria), which show important structural differences, such as average topographic heights, more elevated in the EL, or variable slope angles and deformation rates, both higher in the EL. Using seismological data, Sgroi et al. (2021) observed spatial changes in depth distribution of earthquakes recorded in the Ionian Sea, implying that the IF system constitutes a structural boundary between the two lobes, with changes in thickness of the seismogenic layer.

The AEF represents the main tectonic lineament of a set of NNW-SSE striking faults affecting the WL. The IF and AEF

TABLE 1 | Coordinates of OBSs deployed during the SEISMOFAULTS survey and computed time drift at each instrument. Unfortunately, the OBS4 was not recovered at the end of the experiment.

Instrument ID	OBSH2	OBSH3	OBSH4	OBSH5	OBSH6	OBSH7	OBSH8	OBSH9
Latitude	37°42.22′	37°14.28′	37°00.47′	37°24.55′	37°45.77′	37°41.37′	37°25.91′	37°12.37′
Longitude	15°27.33′	15°30.35′	15°38.79′	15°43.39′	16°02.83′	16°22.49′	16°31.78′	16°07.10′
Depth [m]	1767	2,256	2,330	2,242	1,583	2065	2,671	2,752
Measured drift [ms]	−86.9	479.0	LOST	172.5	−215.0	−438.4	−363.5	447.8
Mission length [days]	371	371		371	371	371	371	402

systems are the most seismically active tectonic features in the region (Totaro et al., 2013; Polonia et al., 2016; Presti, 2020) and the main targets of the SEISMOFAULTS project (Billi et al., 2020).

THE OCEAN BOTTOM SEISMOMETER/ HYDROPHONE (OBS/H) NETWORK

Instrumental Features

An OBS/H network including eight stations was deployed in May 2017 and seven of them were recovered in May 2018 (**Figure 1**; **Table 1**; Billi et al., 2020). Unfortunately, the OBS4 could not be recovered at the end of the experiment. All instruments were designed, assembled and tested at the INGV OBS Lab in Gibilmanna (Sicily). The OBS/H model B used in the SEISMOFAULTS experiment is equipped with a Trillium Compact OBS sensor and a 120-s broadband seismometer with 750 V s/m sensitivity. When the OBS reaches the seafloor, the sensor is dropped from a short height onto the sediments, establishing in this way a good mechanical coupling with the seafloor. The OBS includes a telescopic shield that isolates the sensor from bottom currents. In addition to the seismometer, the OBS includes a hydrophone with a 0.001–5 kHz bandwidth. A Guralp CD24 recorder digitizes and acquires data from both sensors, and stores them in local flash memory along with status information. Sampling frequency was set to 100 Hz during the experiment. The digitizer includes a precision clock, based on a Temperature Compensated Crystal Oscillator (TCXO), synchronized to UTC with a GPS receiver just before the deployment. After recovery, the GPS receiver was connected to the digitizer once again, to measure the clock drift accumulated during the mission. Estimated time drifts were < 0.5 s for all OBS/Hs (detailed time drift for each OBS are reported in **Table 1**), and this linear correction of the time drift was applied to the dataset.

Each OBS/H station was equipped with auxiliary systems operating during deployment and recovery, such as the acoustic release, i.e. an acoustic transponder combined with an actuator, which has the following function. During normal operations, a ballast anchors the instrument to the seafloor. Upon reception of a command through an acoustic link, the acoustic release detaches the ballast and the OBS/H leaves the seafloor reaching the sea surface, where it can be recovered. Some features, such as a flashing light and a radio and satellite beacons, help locating the instruments once at the surface. A cylindrical vessel, rated for 6,000 m depth, houses all the electronics and batteries. A titanium frame supports the vessel holding the instrumentation, the release, the beacons, and some buoys required to control the OBS velocity during descent and ascent.

Before data analysis, a quality check of the collected data showed very few gaps in the data stream, with over 99.9% of valid recordings detected. From March 2nd, 2018, to the end of the experiment, OBS7 showed strong disturbances on Z, N and E channels, not detected by the hydrophone, making the identification of seismic signals very difficult. About 549 Gb of data in GCF (Güralp Compressed Format) were converted in SAC (Seismic Analysis Code) format, organized and stored in a simple filesystem archive.

Deployment Sites

The choice of the OBSs deployment sites (**Figure 1**) was guided by the strategy of monitoring those fault/fault systems considered seismically active or potentially active on the basis of previous geological/geophysical studies (Polonia et al., 2011, Polonia et al., 2016, Polonia et al., 2017a; Gutscher et al., 2016). The choice was also tested against available information on seismic records obtained by the INGV network (CSI catalogue, Castello et al., 2006; the ISB catalogue, Italian Seismic Bulletin, ISIDe Working Group, 2007). Final adjustments in the station's positioning were performed analysing marine geophysical data, such as high resolution multibeam bathymetry and single-channel seismic profiles collected during the oceanographic cruises (e.g., Bortoluzzi et al., 2017). Seafloor structures such as scars and/or submarine landslide deposits, as well as canyon drainages and rocky outcrops were carefully avoided. Areas potentially affected by active gravitative and high-energy sedimentary processes were also excluded. Submarine flat surfaces with fine-grained sediments were preferentially chosen, for an optimal coupling of the stations with the seafloor.

The external boundaries of the OBS network were selected to include major lithospheric faults according to available large-scale structural models of the Calabrian Arc (Minelli and Faccenna, 2010; Polonia et al., 2011, Polonia et al., 2016, Polonia et al., 2017a; Gutscher et al., 2016). Our interest was particularly focused on major out-of-sequence thrust faults (splay faults of Polonia et al., 2011) and on lithospheric discontinuities orthogonally segmenting the accretionary wedge, i.e., the Alfeo-Etna and Ionian fault systems (Polonia et al., 2016; Sgroi et al., 2021). The stations were deployed over an area of about 150 × 100 km with a spacing of ~30 km between stations.

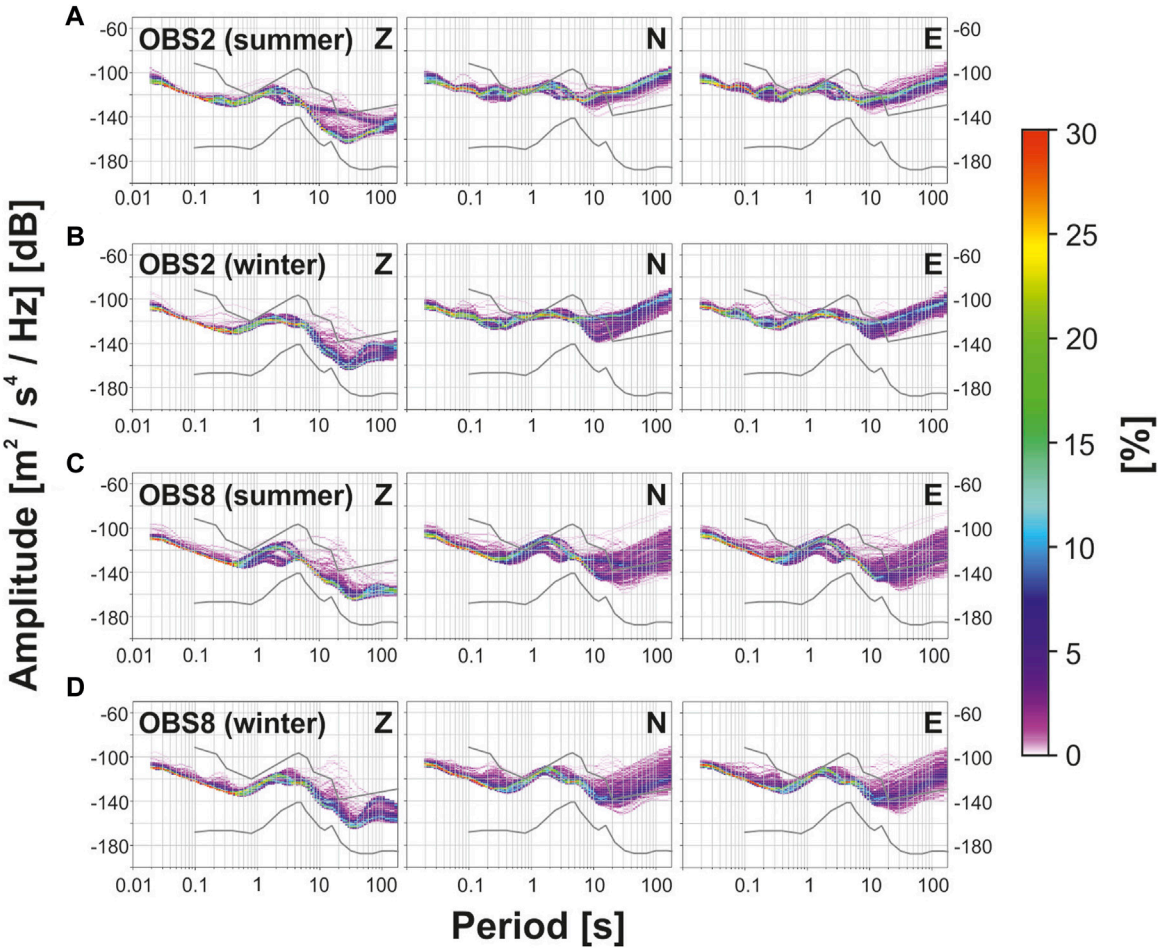

FIGURE 2 | Probability density function (PDF) for the three seismic components (Z, N, E), built during six days in two periods of the year **(A)** OBS2 during 2017, 11–16 July (summer) and **(B)** 2018, 25–30 January (winter) **(C)** OBS8 during the summer and **(D)** winter seasons. The amplitude is given in units of decibels with respect to acceleration (m^2/s^4/Hz). The colour bar represents the probability of occurrence of each PSD normalized from 0 to 30%.

DATA QUALITY

The probability density functions were constructed for the recorded seismic data considering six days in different seasons (**Figure 2**). We used a routine tool for assessing the seismic data quality, using the statistical calculation of the Probability Density Function (PDF). The PDF analysis was performed with the algorithm proposed by McNamara and Buland (2004) and McNamara et al. (2009). Following McNamara and Buland (2004), we constructed the Power Spectral Density (PSD) for data recorded by the sensors during the experiment. Using this technique, the noise-spectra levels are compared with the reference Low Noise Model (LNM) and High Noise Model (HNM) curves obtained by Peterson (1993). The efficient detection of seismic waves and the accurate recognition of seismic phases from all distances are limited by the levels of background noise in different frequency bands of the signal.

Figure 2 shows an example of PDFs calculated on the three seismic components of the OBS2 (**Figures 2A,B**) and OBS8 (**Figures 2C,D**) during six days in two different seasonal times: summer (July 11–16, 2017; **Figures 2A,C**) and winter (January 25–30, 2018; **Figures 2B,D**). The comparison of our results with the LNM and HNM reference curves shows that the noise spectra levels are generally contained within the Peterson (1993) model limits, except for the high noise on horizontal components at low frequency (long period), both in summer and winter times. The fairly high noise levels in the long-period band (>10 s) observed on the horizontal components are due to the sea currents that are an important noise source at the seafloor sites (which tilt the sensor; Webb and Crawford, 2010). The typical microseismic peaks are recognizable: Single Frequency peak (SF), at 10–20 s and the much stronger Double Frequency peak (DF), at about 5 s (Webb, 1998). The SF is generated by non-linear coupling of sea waves and bathymetry, while DF is produced by the interaction of sea gravity waves with the seafloor (Webb, 1998; Webb, 2002). Sometimes the DF peak can split into two peaks: the first at ~5–12 s (LPDF, Long Period Double Frequency) generated in open sea during favourable weather condition and the second peak, of a shorter period ~2–5 s (SPDF, Short Period

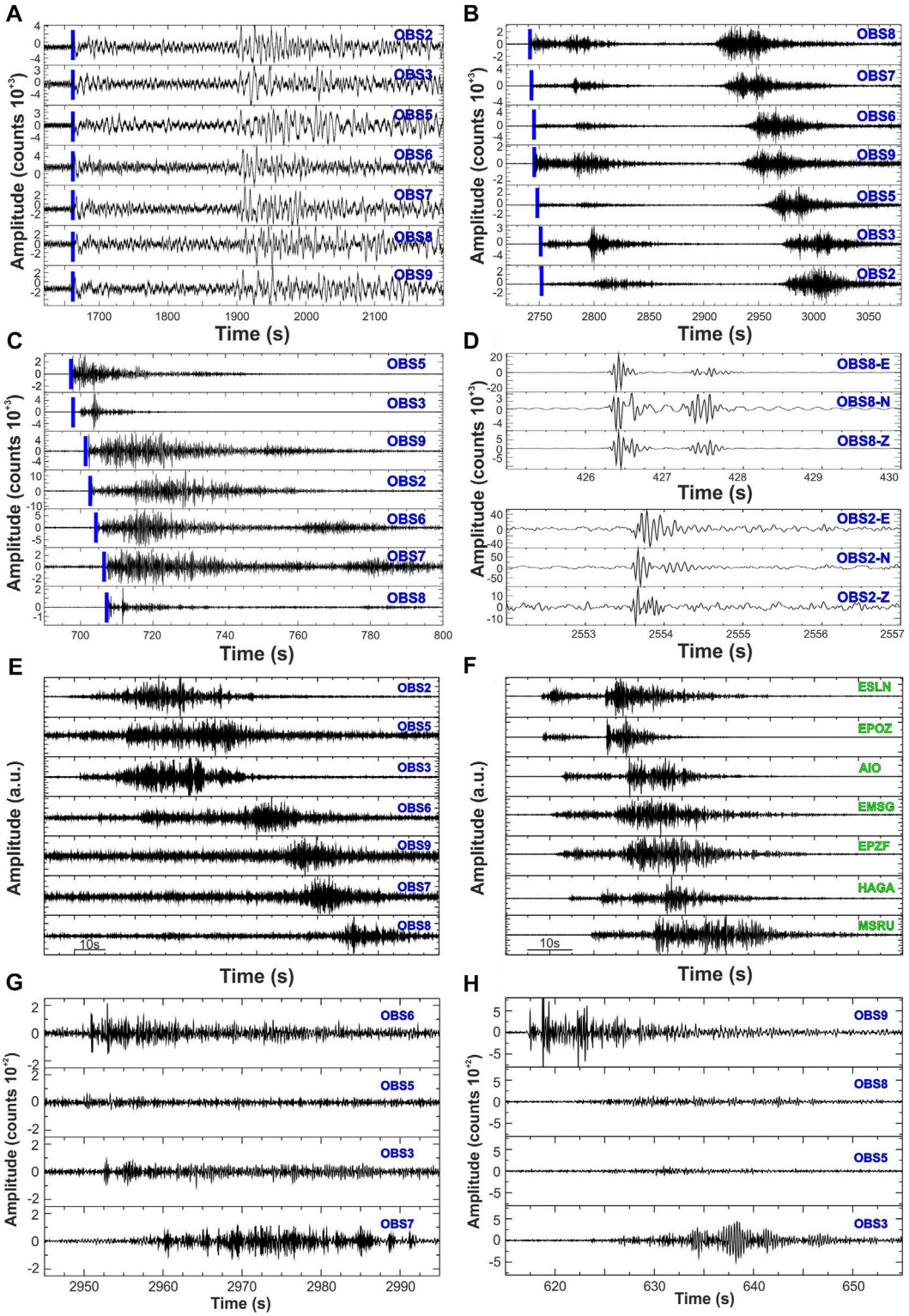

FIGURE 3 | Example of seismic waveforms recorded by the OBS network **(A)** teleseismic event (vertical component, unfiltered; 2018, January 14 h 09:18 UTC M = 7.1 38 km SSW Acari, Perù) **(B)** regional earthquake from Greece (vertical component, 2–12 Hz filtered; 2018, February 21 h 23:44 UTC, M_L = 4.8) **(C)** local earthquake (vertical component, 2–12 Hz filtered; 2017, October 23 h 19:11 UTC, M_L = 3.0); the blue vertical bars on earthquake signals indicate the P-wave arrivals **(D)** Examples of short duration events (three-components, 2–12 Hz filtered) recorded by OBS8 **(up)** and OBS2 **(bottom)**, respectively **(E–F)** Waveforms (vertical components, 2–12 Hz filtered) of an earthquake occurring in the Etna area (2017, June 23 h 20:32 UTC, M_L = 2.2) located by land network (an example of waveforms

(*Continued*)

FIGURE 3 | recorded by land seismic station is shown on right; stations on https://www.fdsn.org/networks/detail/IV/) and that was well-recorded also by most distant OBS (waveforms of marine stations are shown on left) **(G, H)** Examples of waveforms of two earthquakes (vertical component, 2–12 Hz filtered) recorded only by the marine network.

Double Frequency), associated with local windy conditions (e.g. Bromirski et al., 2005).

On the Ionian seafloor, it is possible to observe the splitting of the DF especially during the summer period (e.g., De Caro et al., 2014). In **Figures 2A–C** low noise level during some days around the period range of the SPDF peak is evident. This peak, clearly observed in the summer season, increases in winter time due to a high probability of having frequent windy meteorological conditions. Thanks to the OBS deposition depth, both in summer and winter times, a low anthropogenic noise (short period band <0.2 s) is verified.

The good data quality, also derived from the relatively high recording rate, was checked through comparison with earthquake waveforms recorded by land stations. We found that the OBS stations recorded data from different epicentral distance ranges, i.e., teleseismic, regional, local, and very local events (**Figures 3A–D**), the last ones being recorded solely by the OBS network and not by land stations. **Figures 3E,F** show seismic waveforms (vertical component) of an earthquake located in the Mt. Etna area, associated to the seismic activity of the volcano (2017, June 23 h 20:32 UTC, M_L = 2.2). The location of this earthquake was processed by standard methods in the frame of the monitoring activity by the land network of the Istituto Nazionale di Geofisica e Vulcanologia (INGV). Despite uncertainties in P-and S-phases determination, this event was clearly recorded by the OBS network, also by the most distant stations. Another example concerns an earthquake that occurred in the Ionian Sea (2017, October 23 M_L = 2.8). **Figure 4** shows the picking of P- and S-phases performed on waveforms of land stations and OBSs. The comparison of parameters for the location performed with and without OBSs for this event is reported in **Supplementary Tables 1,2**. Finally, **Figures 3G,H** shows two examples of low-magnitude earthquakes recorded only by the OBS network.

LOCAL EARTHQUAKES

Data collected by OBSs allow us to locate seismic events in the Ionian Sea more accurately, particularly for what concerns hypocentre depth estimates generally affected by large errors due to the lack of an adequate seismic station coverage. Moreover, an intense low-magnitude seismicity often undetected by land stations was recorded (e.g. Sgroi et al., 2007).

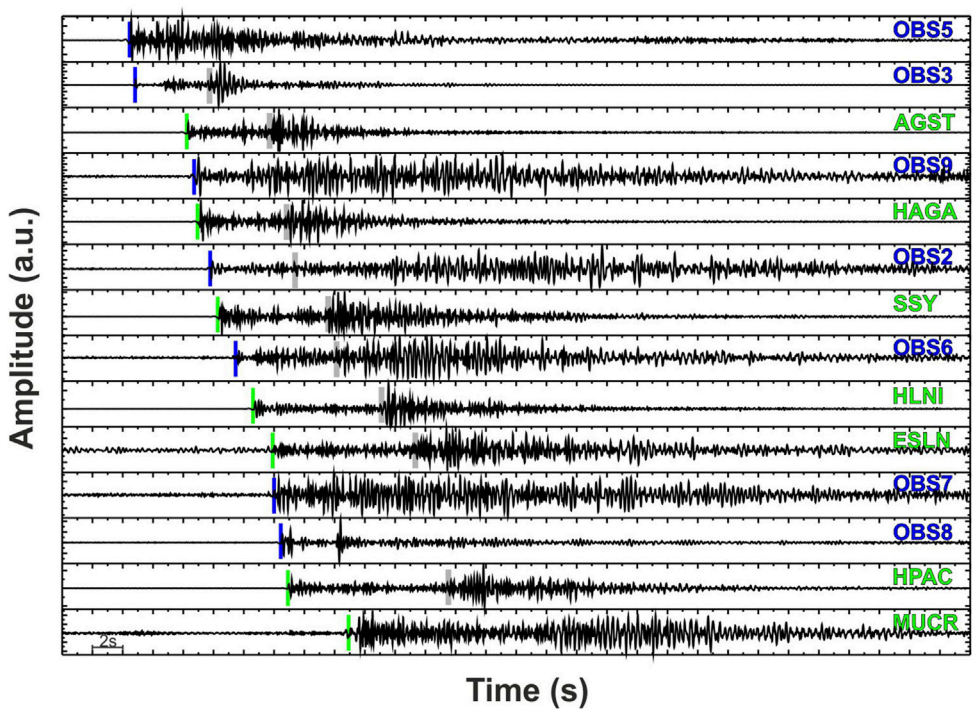

FIGURE 4 | Example of seismic waveform (vertical component) for the local events occurring on October 23, 2017 h 19:11 UTC (M_L = 2.8) and recorded by both land network (a sample of travel times from land stations is represented) and OBS network. The blue and green bars represent the P-phase picked on OBSs and land stations, respectively; grey bars represent the S-phases, picked on horizontal components for both OBSs and land stations. Parameters of location performed with and without the use of OBSs for this event are listed in **Supplementary Tables 1–2**.

The eastern Sicily area is continuously monitored from the seismological and volcanological points of view, due to the presence of active tectonic structures, mostly located offshore, that were the likely sources of large magnitude events in the recent past, and an active volcano, Mt. Etna, which also triggers an intense seismicity. An example of waveforms of a volcano-tectonic earthquake occurring on Mt. Etna and well-recorded by all OBSs is shown in **Figure 3E**, whereas **Figure 3F** shows waveforms of the same event recorded by land stations. However, detailed information regarding tectonic and volcanic structures in the offshore result incomplete when only analysing data derived from the onshore networks, i.e., the National Seismic Network (RSN) and the Etna Regional Network (ERN), both managed by the INGV (INGV Seismological Data Centre, 2006). Currently, the land network (RSN together with ERN) consists of about 90 broadband three-component stations (Trillium 40 s sensors) deployed in Sicily, the Aeolian Islands, and southern Calabria. This network can optimally locate earthquakes occurring on land, but the location of events occurring offshore remains inaccurate. The SEISMOFAULTS OBS network was deployed to mitigate this problem. Here we demonstrate how the network permitted us to find more stable solutions in the earthquake location process for earthquakes occurring offshore.

Local Earthquakes: Integrated Locations

As a first step, we collected available information on earthquake locations, by analysing the seismicity recorded by the land network as reported in the CSI catalogue (Castello et al., 2006), the Italian Seismic Bulletin (Bollettino Sismico Italiano, BSI; ISIDe Working Group, 2007), in the time period covered by the OBSs monitoring.

During the experiment (from May 2017 to May 2018) about 2,400 crustal and sub-crustal earthquakes ($0.4 \leq ML \leq 3.9$) were recorded by the RSN and ERN and located, as reported by the seismic bulletin of the INGV (**Figure 1**). Distribution of these events is non-homogeneous, with the largest clusters clearly linked to the volcanic activity of Mt. Etna. A smaller but relevant cluster of earthquakes is related to seismicity occurring in the southern Tyrrhenian Sea, whereas a smaller number of dispersed seismicity occurred in correspondence of the onshore/offshore transition of the Hyblean plateau and in the external part of the Calabrian Arc in the Ionian Sea. Since our objective was to improve the offshore earthquake location, we concentrated our work on the seismicity that occurred in the Ionian Sea and in the coastal area of eastern Sicily and southern Calabria, by selecting from the land bulletin 133 crustal and sub-crustal events.

After the selection of the events, we looked for them on the OBS seismograms. Then the P- and S-wave arrivals on OBSs were manually picked for these earthquakes (P-phases were determined on the vertical component, while S-phases were picked on the horizontal components). The obtained travel times were added to those from land stations (**Figure 4**) to perform integrated locations. The locations were processed with the tomoDDPS algorithm (Zhang et al., 2009) and a 3D velocity model recently computed for the Ionian Sea (Sgroi et al., 2021). This 3D velocity model derives from a detailed 3D image of the Calabro-Ionian subduction system. The model was obtained by seismic tomography, and shows a Moho depth of about 20 km in correspondence of the OBSs deployment sites. The tomoDDPS software has the advantage of using a combination of both absolute and differential arrival time readings, so that for earthquakes with foci lying close to each other, travel time errors due to incorrect velocity models in the volume outside the cluster will essentially be cancelled. Furthermore, the algorithm can produce a better clustering of earthquakes and, after a few interactions of inversion, a notable residuals reduction of about 43% (from 0.74 to 0.42 s) and 33% (from 0.85 to 0.56 s) is observed for both locations without and with OBS, respectively.

We located the 133 crustal and sub-crustal events with and without the travel times from OBS, and compared the results of the two locations. **Figure 5** shows maps and E-W and N-S sections related to the locations without (**Figure 5A**) and with (**Figure 5B**) data from the OBSs. Although, at first glance, the comparison between relocation with and without OBSs travel times does not show visible differences in the map and on the E-W and N-S sections, they are perceptible in terms of location parameters.

The use of the combined network of land stations and OBSs has improved the earthquake location in terms of horizontal and vertical errors but the most impressive result is the strong decrease of azimuthal GAP. The presence of the marine network allowed us to significantly decrease the Mean (M) and Standard Deviation (SD) values computed on GAP, horizontal (ErrX and ErrY) and vertical (ErrZ) errors (**Figure 6**). As expected, a rough increase of Mean and Standard Deviation (SD) of rms (root mean squares travel-time residual in s) values is observed. As a matter of fact, average rms for all events span from M = 0.24 s (SD = 0.13) of locations without OBSs to 0.36 s (M) of locations with OBSs (SD = 0.17). On the other hand, the consistent decreases in azimuthal gap and on horizontal and vertical errors demonstrate the major stability of the integrated location solutions. Average GAP for the 133 events decreases from M = 207° (SD = 54) of locations without OBSs to M = 131° (SD = 63) of locations with OBSs. Most of the events have consistent decreases of GAP up to 251°. One significant example is the earthquake that occurred on 2017, December 26 ($M_L = 2.3$) and located with OBSs at 37.8805 latitude and 15.44433 longitude (30.91 km depth). The horizontal (ErrX, ErrY) errors of locations without OBSs are characterized by M = 0.44 km (SD = 0.30; ErrX), M = 0.46 km (SD = 0.29; ErrY), while vertical error (ErrZ) shows M = 0.76 km (SD = 0.58). The horizontal errors of the location with OBSs are lower: namely, ErrX is characterized by M = 0.40 km (SD = 0.22) and ErrY has M = 0.34 km (SD = 0.22), while ErrZ is significantly lower and it is characterized by M = 0.46 km (SD = 0.32). In general, differences in the azimuthal GAP can exceed about 76°, while notable reductions of horizontal and vertical errors (up to 1.00 and 1.05 km for the two horizontal errors and 3.26 km for vertical errors) are also observed. A comparison of the parameters obtained in the two cases for an earthquake in the Ionian Sea is reported in **Supplementary Tables 1–2**, which report the results of the 133 locations performed without and with OBSs travel times, respectively.

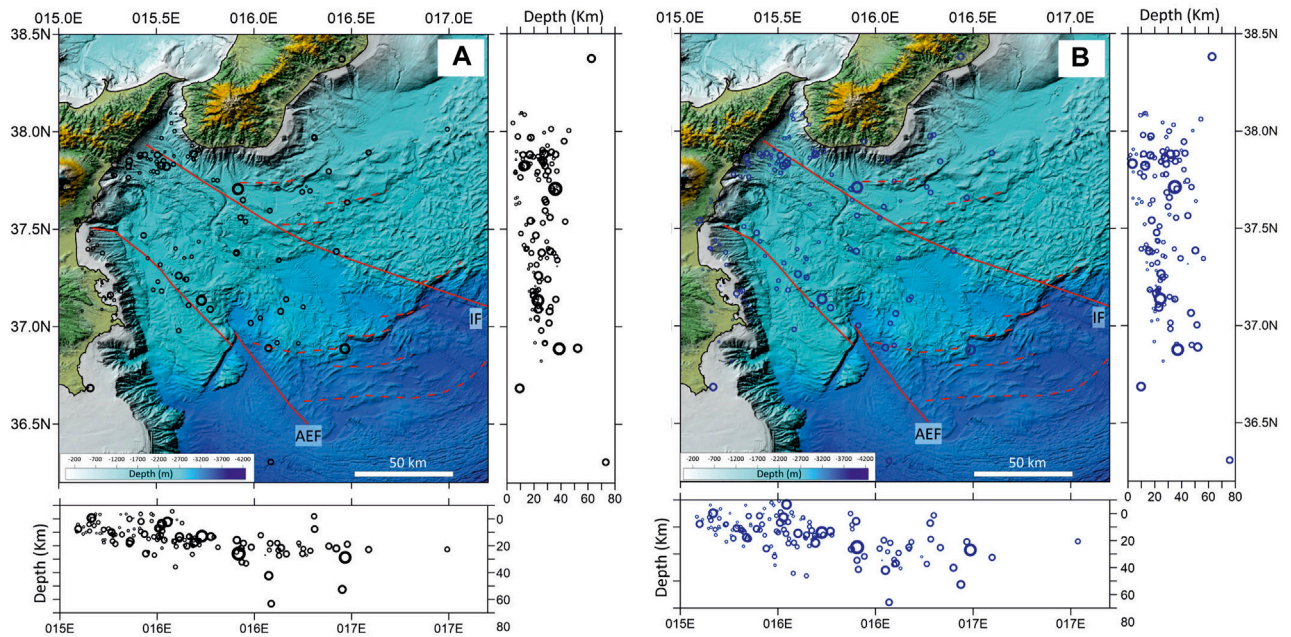

FIGURE 5 | Maps and E-W and N-S sections of 133 earthquake relocations based on a previous 3D velocity model (Sgroi et al., 2021) and computed **(A)** without OBSs travel-times (black circles) and **(B)** with OBSs travel-times (blue circles). The circle sizes are proportional to the M_L as reported on land seismic bulletin. Parameters of location performed with and without the use of OBSs are listed in **Supplementary Tables 1–2**. Red lines indicate the position of Alfeo-Etna fault (AEF), Ionian fault (IF) and splay faults (**Supplementary Tables 1,2,3**). Bathymetric map was obtained from high resolution multibeam collected during the oceanographic cruise of SEISMOFAULTS project (Cuffaro et al., 2019; Billi et al., 2020) and merged with DEMs from https://portal.emodnet-bathymetry.eu/.

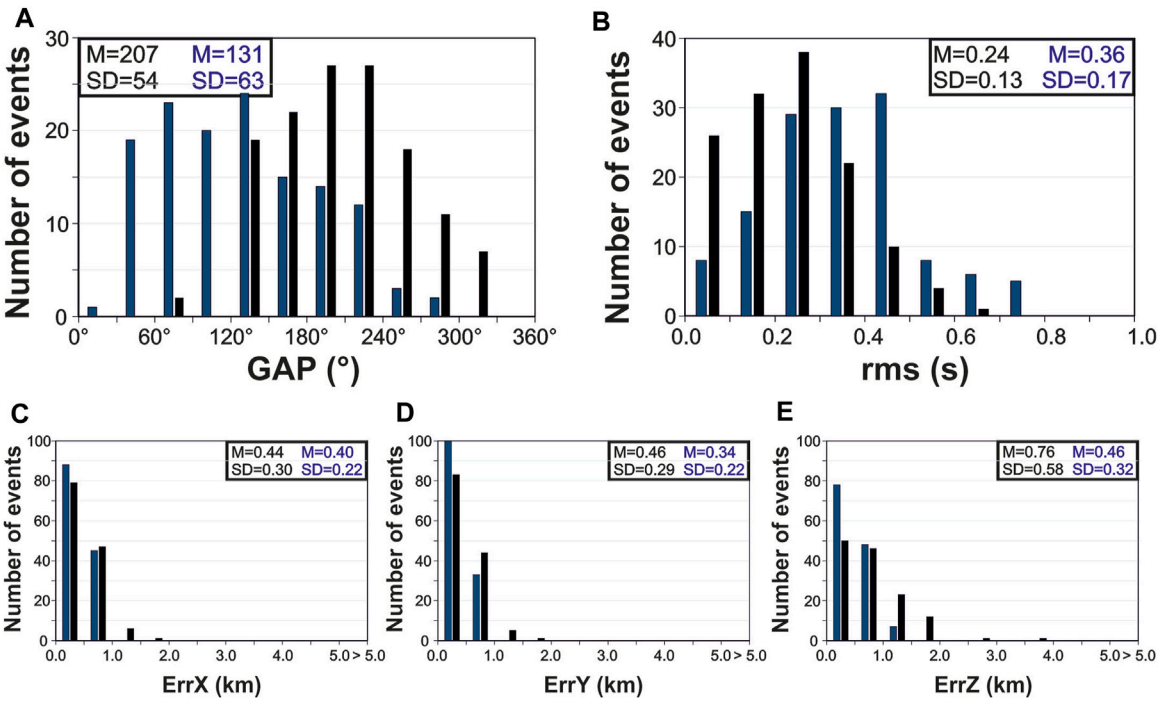

FIGURE 6 | Statistical analysis in terms of Mean (M) and Standard Deviation (SD) values computed on GAP **(A)**, rms **(B)**, and **(C, D, E)** horizontals (ErrX, ErrY), and vertical (ErrZ) errors for location with OBS travel times (blue histograms) and without OBS travel times (black histograms). The presence of an offshore network contributed to an improved relocation quality.

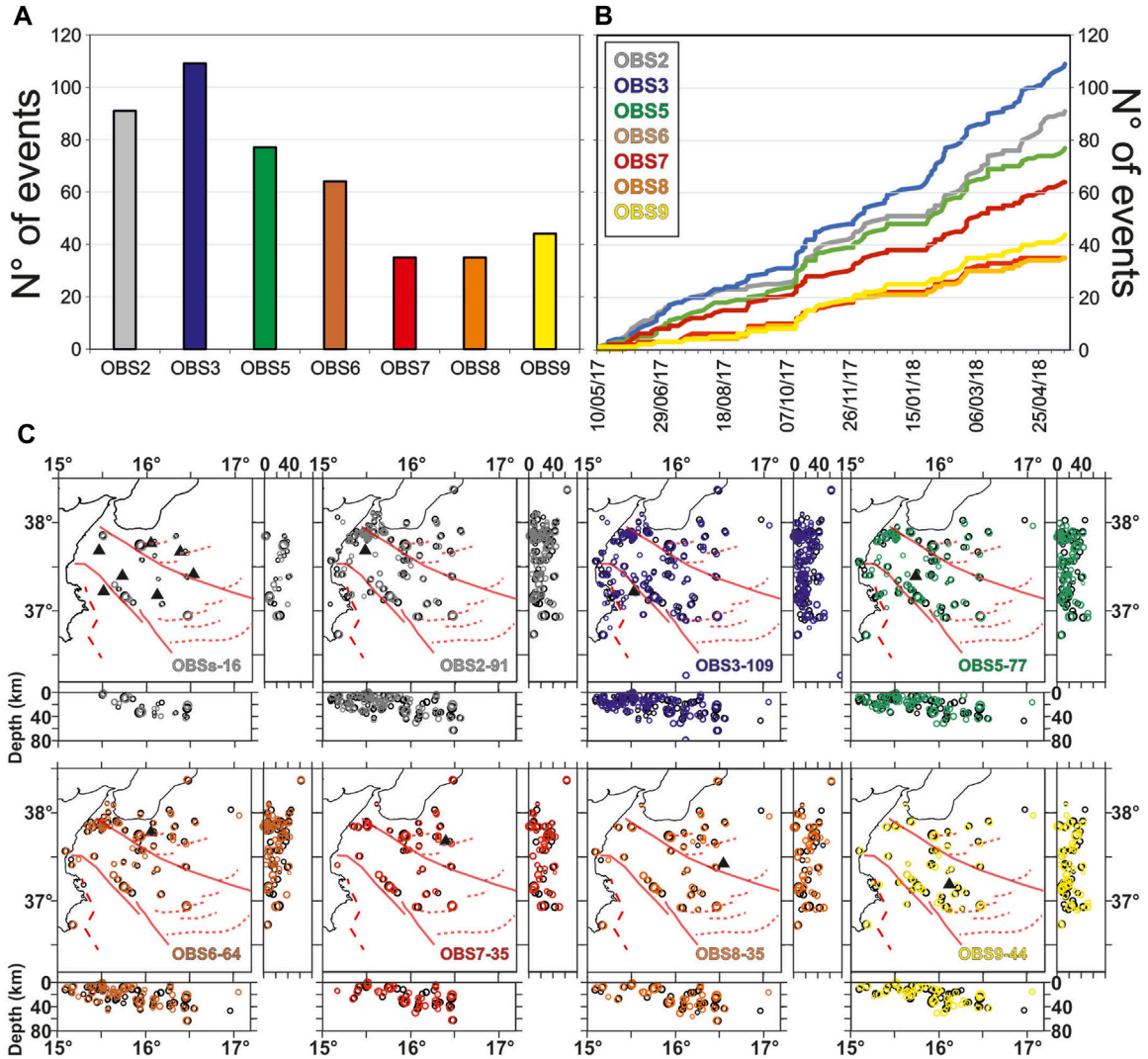

FIGURE 7 | Detection efficiency of the OBS network for 133 local earthquakes located through the integration of travel times by marine and land stations **(A)** Histograms and **(B)** occurrence in time of the number of earthquakes recorded at each OBS **(C)** Maps and E-W and N-S sections of earthquakes recorded by each OBS. Main geological features including the Alfeo-Etna Fault and Ionian Fault (Polonia et al., 2016) and the Malta Escarpment are sketched in red.

TABLE 2 | Number of integrated locations (on 133) of earthquakes recorded both by land and OBS stations, locations (on 76) of low-magnitude earthquakes recorded only by the OBS network, earthquakes and SDE recorded at the single OBS station. The asterisk in OBS7 indicates that this computation is up to 2018 February 28.

	OBS2	OBS3	OBS5	OBS6	OBS7	OBS8	OBS9
Local earthquakes	91	109	77	64	35	35	43
Low-magnitude earthquakes	50	65	61	63	49	42	51
Single OBS earthquakes	46	486	148	23	72*	579	110
SDE	614	3,136	1,246	339	1,022*	2,681	904

We now consider the detection capability of the OBS network. A group of 16 earthquakes (on a total 133 integrated locations) were recorded at all OBS stations (1.9 $\leq M_L \leq 3.8$). Since most of the earthquakes are near the eastern Sicily coast, OBS3 recorded the largest number of events (**Figures 7A,B**; **Table 2**). Histograms detailing the number

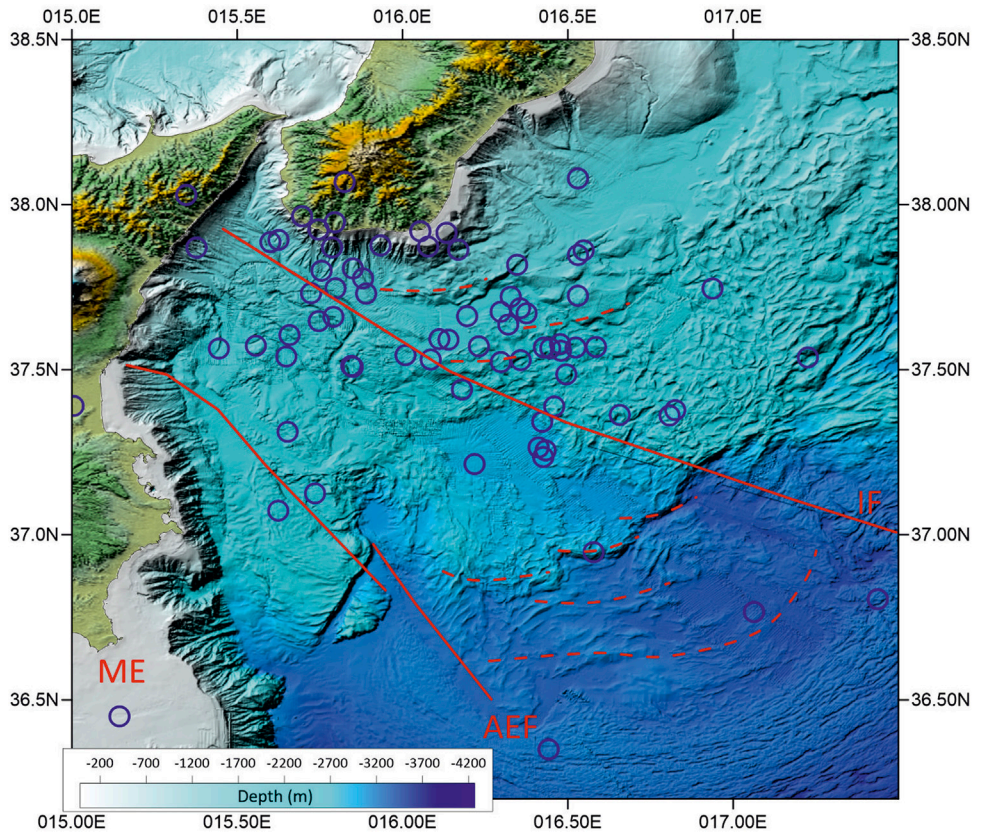

FIGURE 8 | Distribution of epicentres of the 76 earthquakes recorded only by the OBS network. Parameters of location for these events are listed in **Supplementary Table 3**. The main tectonic structures including the Alfeo-Etna Fault and Ionian Fault (Polonia et al., 2016) are sketched in red. Bathymetric map was obtained from high resolution multibeam collected during the oceanographic cruise of SEISMOFAULTS project (Cuffaro et al., 2019; Billi et al., 2020) and merged with DEMs from https://portal.emodnet-bathymetry.eu/.

of located earthquakes (on 133) for each OBS as well as maps and E-W and N-S sections of locations (with and without travel times from OBSs) are shown in **Figures 7A–C**. In **Figure 7C** the shift between the two locations (with and without OBS) can be observed. Major differences are evident for the most external areas of the Ionian basin where the gap of seismicity exists. This gap is due to the fact that the land network alone is not able to cover the hypocentres well. On the other hand, differences are visible also in certain onshore and coastal areas that are characterized by high values of shift, as for example in correspondence of the Hyblean Plateau, Etna offshore and the Messina Strait.

Local Earthquakes: Low-Magnitude Event Locations and Single Station Events

The Ionian Sea tectonic structures are a source of significant microseismicity, mostly undetected by the land network. As an example, the NEMO-SN1 seafloor observatory deployed about 25 km offshore Catania, recorded more than 400 earthquakes not present in the bulletins of land stations during the 2002–2003 Etna eruption (Sgroi et al., 2007). This occurrence was considered an additional opportunity for the SEISMOFAULTS experiment to contribute with new microseismicity records to the long-lasting discussion about seismic hazards in the area.

An in-house STA/LTA algorithm, applied to the OBS vertical component, was tuned to automatically detect local seismic events not identified by land stations. As a few thousands of triggers were revealed, a software code was compiled aiming to select records probably including events detected by two or more OBSH, and to organize relative waveforms in individual directories. Finally, waveforms in each directory were manually picked by analysts to identify body-wave arrivals associated to the same earthquake and used for event location.

From the total list of triggers, we removed the travel times related to the earthquakes reported on the local and regional seismic catalogues, obtaining more than 1,600 events not detected by land stations (**Table 2**). About 1,400 events were recorded only at the single OBS while more than 230 earthquakes were contemporaneously recorded by at least three OBSs. For 236 earthquakes recorded by at least three OBS, we attempted a location, using the tomoDDPS algorithm (Zhang et al., 2009) and a recent 3D velocity model computed in the western Ionian area (Sgroi et al., 2021) that well represent the pattern of the tectonic structures in terms of velocity and depth layers.

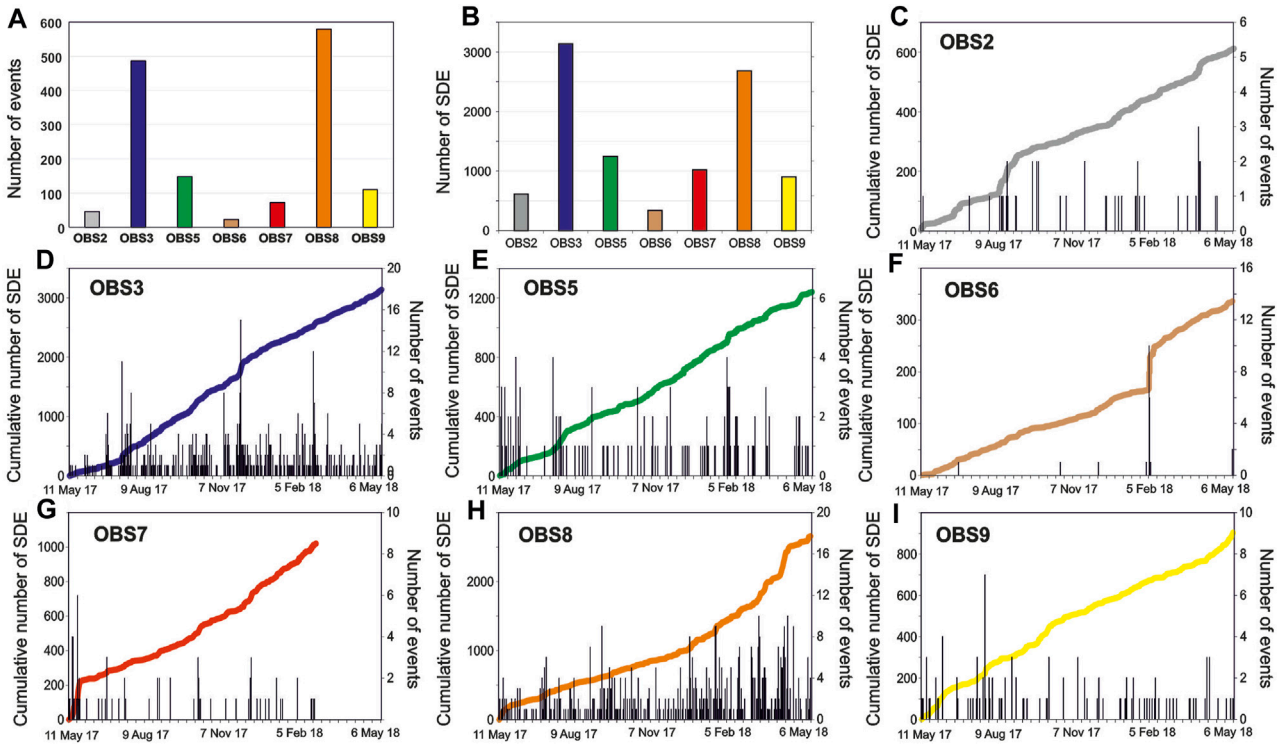

FIGURE 9 | (A) Histograms of the number of single station earthquakes recorded only by the single OBS **(B)** Histograms of the number of SDE recorded by the single OBS **(C–I)** Comparison between the number of SDE and the number of single station events recorded at each OBS.

We manually picked P- and S- phases (as described above) and a location was attempted for events recorded at least at three OBSs and having a minimum of 6 phases. Identifying seismic phases is somewhat more difficult for OBSs (**Figures 3G,H**). This is partially due to the relatively weak coupling of the instrument with the poorly consolidated, water-saturated sediment environment, and above all it is due to the low-magnitude of events. Non-ideal coupling leads to damping of the seismic signals, which strongly attenuate the amplitudes at higher frequencies. As an example, **Figures 3G,H** show the waveforms of two events recorded and located only by the OBS network. Few events were recorded at several OBSs (as for the example shown in **Figures 3G,H**), but in most cases the earthquakes were recorded by at most three or four OBSs. These low-magnitude local events, having low energy, generate waves that attenuate within a few tens of kilometres, as testified by the recorded amplitude of waveforms. As reading the S-phases was very difficult, the depth of events is not reliable in most cases. Moreover, since the seismicity recorded by OBSs only was of low magnitude, also the spacing of the OBS network, preclude an accurate location of the events. In spite of these problems, we were able to locate 76 "new" earthquakes. The distribution of locations by OBS is shown in **Figure 8** (location parameters are reported in **Supplementary Table 3**). The distribution of seismicity is well related with the pattern of tectonic structures that exist in the Ionian Sea. Small clusters are identified, and, in particular, three south of Calabria are well correlated with the tectonic structures proposed by Polonia et al. (2016), whose state of activity was evidenced by Sgroi et al. (2021).

A high number of events was recorded only at the single OBS. Histograms of **Figure 9A** show the number of single station events. The seafloor stations that recorded the highest number of events were the OBS3 (486 earthquakes) and the OBS8 (579 earthquakes), whereas the minimum number of events were recorded by the OBS6 (23 events only). As these low-magnitude events are recorded at the single station, it is reasonable that their sources are within the semi-interspacing between two adjacent OBS (about 15 km). Due to the large multitude of single station earthquakes, it is our intention to implement an automatic system of detection and classification of seismic signals of various kinds recorded only by the OBS stations and to better identify the seismogenic source, as proposed by Sánchez-Reyes et al. (2021) for the Balsorano seismic sequence. Although we do not perform an extensive data analysis in this work, the distribution of number of events on each OBS is indicative of the state of seismic activity associated to the tectonic structures.

Short Duration Events

Our dataset includes a large number of short, impulsive signals which, in the literature are defined as Short Duration Events (SDE; **Figure 4**). These kinds of signals are currently detected at the seafloor in different parts of the world, and they have been associated with several possible sources, including fluid-filled cracks in sedimentary basins (Diaz et al., 2007), gas seepages along active faults (Tary et al., 2012; Embriaco et al., 2014), or even due to biological activity (Buskirk et al., 1981;

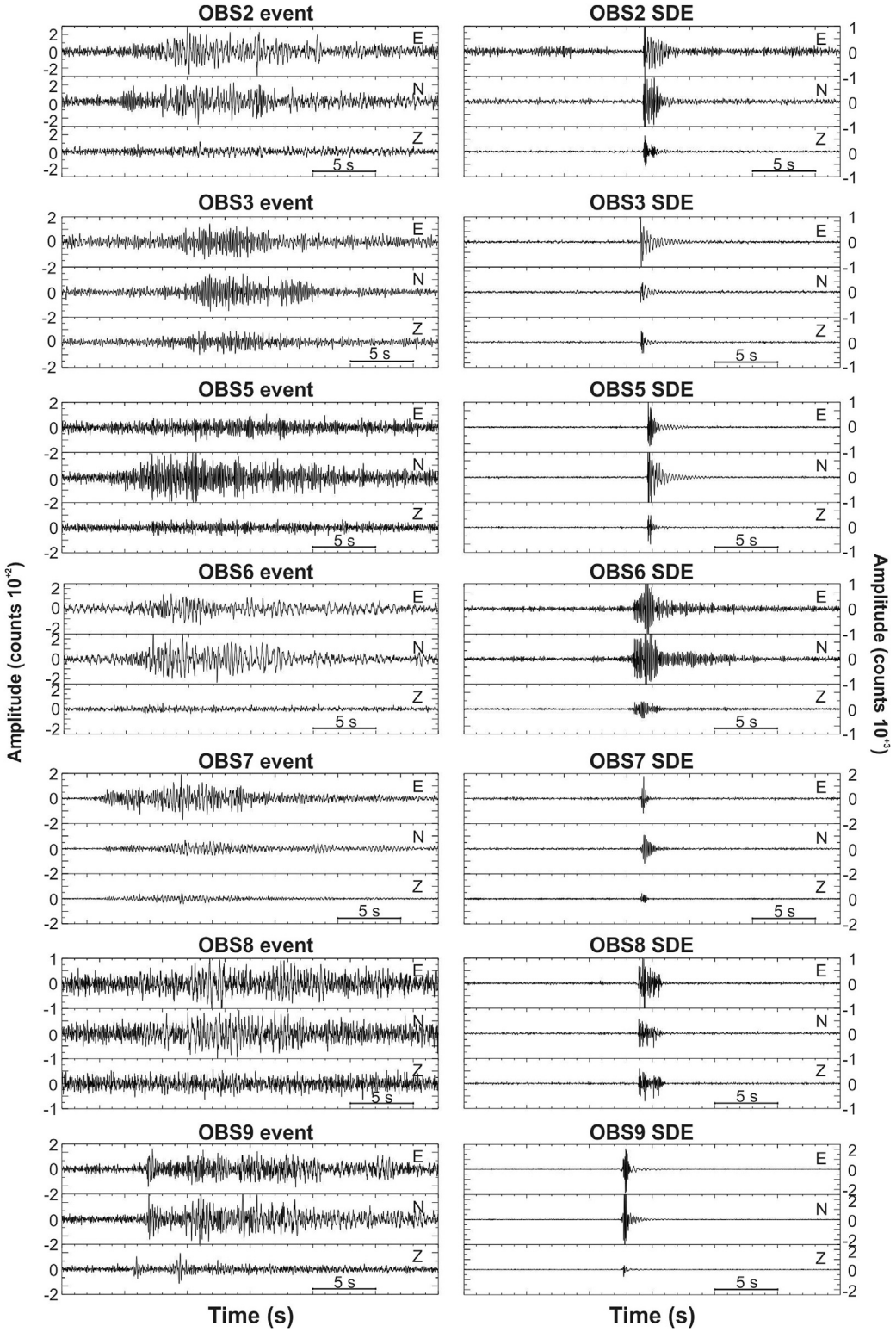

FIGURE 10 | Comparison between waveforms (three components) of earthquakes **(left)** and SDEs **(right)** recorded at the single OBS. Time window is 30 s long for both signals and all records were filtered with band-pass Butterworth filter in the same frequency range 2–25 Hz.

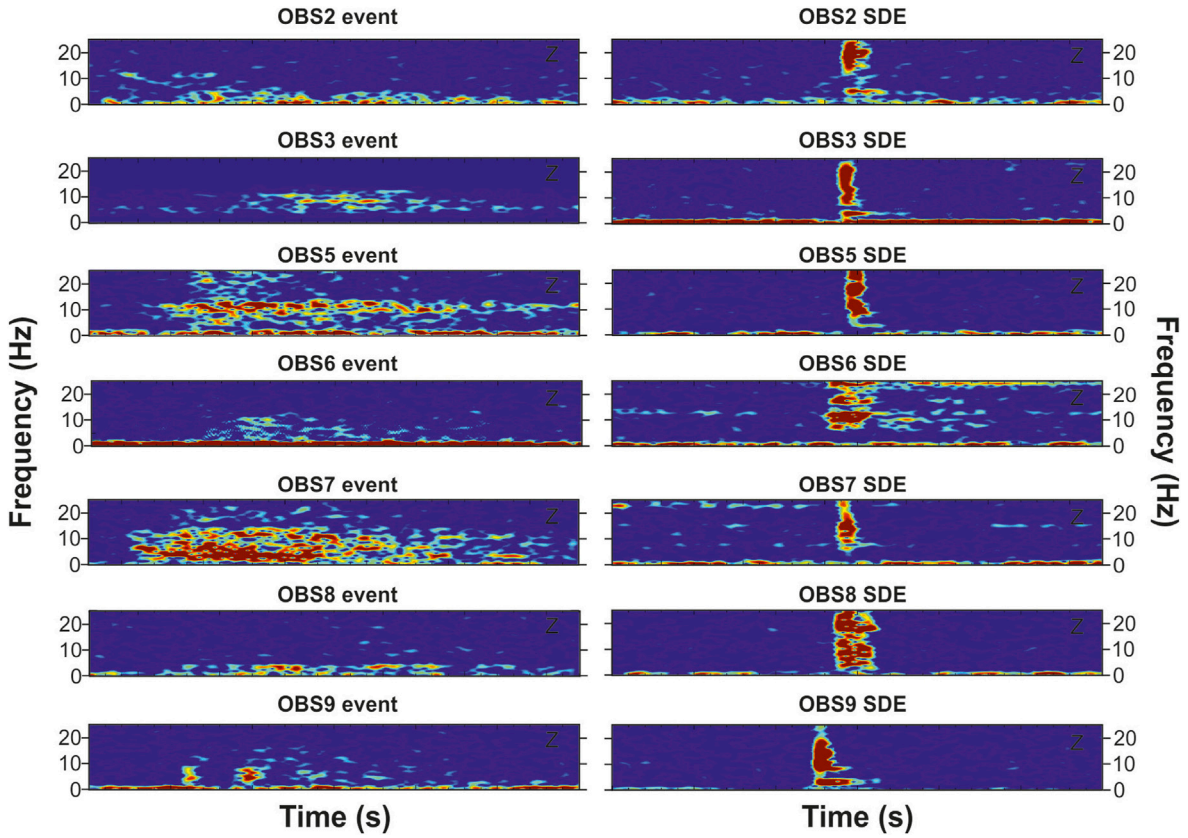

FIGURE 11 | Spectrograms computed on vertical component of earthquakes **(left)** and SDEs **(right)** recorded at the single OBS. Records were filtered with band-pass Butterworth filter in the frequency range 2–25 Hz. Colours of spectrograms are in log(counts ^{2}/Hz) units and represent distribution of energy of the recorded signals as a function of time (*x* axis) and frequency (*y* axis). Warm colours (red, yellow and green) define the dominant spectral amplitudes; cooler colours (light to dark blue) define lower spectral amplitudes and background.

Bowman and Wilcock, 2014). In general, SDEs are ascribable to hydraulic micro-fracturing processes, such as pressure transients generated by fluid-filled cracks (Diaz et al., 2007), and they have been best described in hydrothermal and volcanic (e.g., Sohn et al., 1995), as well as tectonic (e.g., Embriaco et al., 2014) systems. Moreover, such a small seismicity shows similarity with slow-slip events associated to a shear zone with low-friction (e.g., Matsuzawa et al., 2010) that occur in the deeper extents of areas where large earthquakes are expected in subduction zones. In the Ionian Sea, Sgroi et al. (2014) showed that SDE signals recorded by the NEMO-SN1 seafloor observatory could result from hydrofracturing induced by magmatic activity around Mt. Etna.

During the one-year-long SEISMOFAULTS experiment, about ten thousand of SDEs (**Table 2**) were recorded by the OBS network, whose detection in correspondence of the single OBS is reported in **Figure 9B**. As the number of SDEs and their waveforms varied on each OBS (**Figure 10** shows examples of SDE waveforms recorded at the single OBS), it is reasonable to think that their origin process may be different, depending on the position of the seafloor station. In general, SDEs (**Figures 4**, **10**) are characterized by sharp waveforms, high-frequency content (from about 1 Hz up to 50 Hz; **Figure 11**), and very short duration (about 2 s). Moreover, this signal rapidly attenuates as the wave travels, and this points to the small scale of the SDE generation process and to a nearby source.

As for the single station events, the OBSs that recorded the highest number of SDEs were OBS3 (3,136) and OBS8 (2,681), while the lowest number is observed on OBS6 (339). The detection of SDEs by the OBSs varies in time and occurs in clusters in time. A direct proportionality between the occurrence of SDE and single station events is observed on all OBSs (**Figure 9**). The most impressive relation between SDE and low-magnitude events is visible on the OBS6 (due to its lower number of these events) that shows a time distribution of SDE characterised by the occurrence of a small swarm of 69 SDE in the period 2018, February 4–7 (**Figure 9F**). Moreover, the waveforms of SDE signal recorded at the OBS3-OBS5-OBS7-OBS9 (**Figure 10**) show similitude with signals conducible to microfracturing processes, while SDEs recorded at the OBS2-OBS6- OBS8 are almost different from the same signal recorded by the former OBS stations, showing typical features of cracks associated to gas seepage variations (Franek et al., 2017). The same groupings are well defined when comparing spectrograms computed on both events and SDE recorded at the single station (**Figure 11**).

We cannot accurately locate the SDE source since we only have data from one seismic station: as demonstrated in previous studies performed in other areas, the SDE source distance from the sensor is estimated in the order of hundreds of meters (Sultan et al., 2011), or even tens of meters (Tary et al., 2012), whereas their amplitude is roughly higher than the one of single station earthquakes (see amplitude values in **Figure 10** for single station events and SDE) and their distribution is indicative of the state of activity of structures placed in the Ionian Sea. As differences in the waveforms and spectrograms of SDE are also observed at each OBS (**Figures 10**, **11**), we can argue that different processes generate these signals.

The distribution of SDEs recorded during the SEISMOFAULTS experiment could be associated with active tectonic and volcanic processes, also demonstrated by the good correlation between the occurrence of events and the occurrence of SDEs, both recorded by the single OBS (**Figures 9C–I**). This comparison shows that the increase in the number of SDEs coincides with the occurrence of a higher number of earthquakes in the same time period recorded at the single OBS.

DISCUSSION AND CONCLUSIONS

Prior to the SEISMOFAULTS experiment, available seismological data, collected both by onshore seismic station and by the NEMO-SN1 seafloor observatory (Sgroi et al., 2021), have shown that the submarine Calabrian Arc is characterized by a pattern of small magnitude, scattered earthquakes, mainly due to slow rates of NW-directed Ionian subduction. The new data acquired during the SEISMOFAULTS project show a significant number of seismic events not detected by the land stations (**Figure 8**) that could provide a more complete picture of the active seismicity in the region. Integrated analyses of OBSs and land stations data show that seismicity is mostly located off southern Calabria and Taormina, in southeastern Sicily, where a dense cluster of events was recorded, as well as south of Catania. A diffuse seismicity pattern characterizes the central Ionian Sea, the alleged site where most active tectonic features of the submerged part of the Calabrian Arc are located.

The OBSs that have recorded the largest number of events are those located close to Mt. Etna (OBS2), where seismic activity is mostly related to fluids associated to volcanism and across the AEF (OBS3 and OBS5 in **Figure 1**). Together with OBS3 and OBS5, also OBS8 shows a larger number of SDE events, which are possibly related to fracturing triggered by fluid flows (Franek et al., 2017). This occurrence suggests a likely relationship between fluid flow and tectonics since these OBSs are close to the AEF and IF systems that were described, based on independent geophysical data, as seismogenic structures (Polonia et al., 2011). We cannot exclude that the increased number of events recorded by these OBSs might be related to their deployment sites characterized by flat regions surrounded by relatively wide sedimentary basins, favouring an optimal coupling between instrument and seafloor, and decreasing their detection thresholds. This observation confirms the need for a careful site selection for the OBS deployment, avoiding actively deforming areas, canyons, and submarine landslides, which can be achieved thanks to a close cooperation between seismologists and geologists.

Figure 9A shows the number of low-magnitude earthquakes recorded by the OBSs. The distribution of these events roughly mimics the IF trend, which marks the SW boundary of a crustal block in the Calabrian Arc (EL), where earthquakes are more clustered (**Figures 5**, **8**). This agrees with a more intense deformation offshore southern Calabria, as also shown by analysis of multichannel seismic reflection profiles (Polonia et al., 2011) and by seismological observations (Sgroi et al., 2021). South of 37.4° latitude, the low-magnitude earthquakes detected by the OBS network are located to the SW of the Ionian Fault and might correlate with tectonic activity along the out-of-sequence thrust faults (**Supplementary Tables 1,2,3**) bounding the landward limit of the external accretionary wedge, which is made primarily of evaporites (Polonia et al., 2011). At the contact between the salt-bearing wedge and the inner clastic wedge, splay faults develop and accommodate such rheological change.

The distribution of cumulative recorded events (**Figures 5**, **8**) allows us to unravel the connection between seismicity and active tectonics. Moving from W to E along the accretionary wedge of the Calabrian Arc, we recognize different clusters of earthquakes with different characters.

The seismic events observed close to the Eastern Sicily coast are shallow, occurring within a depth interval <20–22 km, which correspond to crustal levels of the upper plate, in agreement with a Moho depth of about 20 km in this area (Sgroi et al., 2021). Some of these events might be correlated with the Mt. Etna activity, while those to the south might correlate with the Malta Escarpment, which appears tectonically active north of Siracusa (**Figure 1**).

The largest magnitude events (**Figure 5**) appear to correlate with the major fault systems, i.e., the AEF, the out-of-sequence splays **Supplementary Tables 1,2,3**, and the IF. These structures were described as source regions for major historical earthquakes based on structural maps and paleoseismological data (Polonia et al., 2012; Polonia et al., 2017b). A number of seismic events are concentrated along the AEF and occur at greater depth >30 km implying a seismogenic thickness larger than those close to the ME. The greater hypocentral depth is reached by earthquakes along the IF and splay faults where the seismogenic layer appear to be from 30 to 60 km thick. The earthquakes located in the more external region, in particular, have depths of 40–60 km, suggesting that they might be related to the lower underplating African plate. Most epicentres fall within the deformation band associated to the Ionian Fault that seems to be the most seismically active feature in the studied area together with a parallel fault a few kilometers to the south of the Ionian Fault. It is remarkable that the Ionian Fault is particularly active (seismically) at its northwestern tip that is only a few kilometers to the south of the Messina Straits. This tip activity is interesting as it could potentially activate, in the future, extensional earthquakes in the Messina Straits according to the wing fracturing process proposed by Sgroi et al. (2021). The Messina Straits, in fact, occupies the extensional quadrant at the northwestern tip of the right-lateral transtensional IF (Polonia et al., 2016) in the region characterized by differential rollback of the Ionian subduction (Doglioni et al., 2001).

We observe widespread seismicity to the north of the Ionian Fault near the southern coast of Calabria. We cannot ascribe this seismicity to a tectonic domain with certainty; however, the presence in that region of seismically active shortening (Sgroi et al., 2021) allows us to hypothesize that this seismicity may be linked to the compressive structures described through geophysical data (Polonia et al., 2011).

The occurrence of SDE events and their close correlation with the occurrence of microseismicity could indicate significant contamination of the bottom waters from saline (evaporate-type) CH4-dominated crustal-derived fluids. These were observed in the Ionian Sea, in correspondence of a mud volcano (the Bortoluzzi Mud Volcano; BMV) discovered during the SEISMOFAULTS cruise in May 2017 (Cuffaro et al., 2019). The BMV is one of many mud volcanoes offshore Calabria. It is therefore reasonable to suppose that the origin of SDE recorded by OBS6 and OBS8 may be associated to active geofluid venting. For the OBS2 the association of SDE source mechanisms to fluids linked to Mt. Etna volcanism is also conceivable. On the other hand, OBS3-OBS5-OBS7-OBS9 show similarities with signals conducible to microfracturing processes.

In synthesis, one year of recording by a network of seven OBS in the Ionian Sea shows the seismic activity of the most important tectonic features of the study area, including the Ionian Fault and other transverse faults across the Calabrian Arc such as the Alfeo-Etna Fault and the Malta Escarpement. Active thrusting may also occur off southern coast of Calabria pointing for active subduction processes along the Ionian slow convergent system.

DATA AVAILABILITY STATEMENT

The original contributions presented in the study are included in the article/**Supplementary Material**, further inquiries can be directed to the corresponding author.

Waveform data of earthquakes recorded by the INGV stations (land stations) are available online from the European Integrated Data Archive (EIDA) at http://eida.rm.ingv.it.

P- and S-phase arrival times associated to earthquakes occurred in the Ionian basin and analysed in this study are available online in the database ISIDe (Italian Seismological Instrumental and parametric Data-base; http://cnt.rm.ingv.it/iside). The catalogues of all located earthquakes published in this study are available in the **Supplementary Material**.

AUTHOR CONTRIBUTIONS

TS conceived and designed the original idea of the study. TS, AP, and ABo wrote the manuscript and prepared figures. AC, GD'A, GF designed, assembled, and tested the OBS stations. TS, MCa, MN, FF, SM, CM, LP, PP, SP, AU analysed the data. LB, ABi, MCu, LG, CM, SM, AU, and CD contributed in the revision of the manuscript and the figures.

ABi, AP, MCu, TS, LB, GD'A, LG, and CD conceived and coordinated the SEISMOFAULTS experiment, from which this study derives.

FUNDING

The OBS experiment complements the characterisation of a key area hosting the Western Ionian Sea Facility of EMSO research Infrastructure (www.emso.eu) of which NEMO-SN1 is one of the observation components. The SEISMOFAULTS experiment was partially supported by the Italian Ministry of University and Research in the framework of Italian participation to EMSO.

ACKNOWLEDGMENTS

Thanks to Stephen Conway for revising the English form of the manuscript. We also wish to acknowledge the Guest Associated Editor Susan Bilek and the insightful and constructive reviews of two reviewers.

SUPPLEMENTARY MATERIAL

The Supplementary Material for this article can be found online at: https://www.frontiersin.org/articles/10.3389/feart.2021.661311/full#supplementary-material

REFERENCES

Argnani, A., and Bonazzi, C. (2005). Malta Escarpment Fault Zone Offshore Eastern Sicily: Pliocene-Quaternary Tectonic Evolution Based on New Multichannel Seismic Data. *Tectonics* 24, TC4009. doi:10.1029/2004TC001656

Bianca, M., Monaco, C., Tortorici, L., and Cernobori, L. (1999). Quaternary normal Faulting in southeastern Sicily (Italy): a Seismic Source for the 1693 Large Earthquake. *Geophys. J. Int.* 139, 370–394. doi:10.1046/j.1365-246x.1999.00942.x

Billi, A., Cuffaro, M., Beranzoli, L., Bigi, S., Bosman, A., Caruso, C., et al. (2020). The SEISMOFAULTS Project: First Surveys and Preliminary Results for the Ionian Sea Area, Southern Italy. *Ann. Geophys.* 63. doi:10.4401/ag-8171

Bortoluzzi, G., Polonia, A., Torelli, L., Arton, A., Carlini, M., Carone, S., et al. (2017). Styles and Rates of Deformation in the Frontal Accretionary Wedge of the Calabrian Arc (Ionian Sea): Controls Exerted by the Structure of the Lower African Plate. *Ital. J. Geosci.* 136, 347–364. doi:10.3301/ijg.2016.11

Boschi, E., Guidoboni, E., Ferrari, G., Valensise, G., and Gasperini, P. (1997). *Catalogue of the strong Earthquakes in Italy from 461 BC to 1990.* Bologna: ING. & SGA, 973.

Bowman, D. C., and Wilcock, W. S. D. (2014). Unusual Signals Recorded by Ocean Bottom Seismometers in the Flooded Caldera of Deception Island Volcano: Volcanic Gases or Biological Activity? *Antartic Sci.* 26, 267–275. doi:10.1017/S0954102013000758

Bromirski, P. D., Duennebier, F. K., and Stephen, R. A. (2005). Mid-ocean Microseisms. *Geochem. Geophys. Geosyst.* 6, Q04009. doi:10.1029/2004GC000768

Buskirk, R. E., Frohlich, C., Latham, G. V., Chen, A. T., and Lawton, J. (1981). Evidence that Biological Activity Affects Ocean Bottom Seismograph Recordings. *Mar. Geophys. Res.* 5, 189–205.

Carminati, E., Lustrino, M., and Doglioni, C. (2012). Geodynamic Evolution of the central and Western Mediterranean: Tectonics vs. Igneous Petrology Constraints. *Tectonophysics* 579, 173–192. doi:10.1016/j.tecto.2012.01.026

Carminati, E., Petricca, P., and Doglioni, C. (2020). "Mediterranean Tectonics," in *Encyclopedia of Geology* (Amsterdam: Elsevier).

Castello, B., Selvaggi, G., Chiarabba, C., and Amato, A. (2006). *CSI Catalogo Della Sismicità Italiana 1981–2002*. Versione 1.1. Roma: INGV-CNT.

Catalano, R., Doglioni, C., and Merlini, S. (2001). On the Mesozoic Ionian basin. *Geophys. J. Int.* 144, 49–64. doi:10.1046/j.0956-540x.2000.01287.x

Chang, E. T. Y., Hsu, S. K., and Lee, C. S. (2008). Earthquake Swarm Recorded by an Ocean Bottom Seismic Array in Southwest Offshore of Taiwan in October, 2005. *Terr. Atmos. Ocean. Sci.* 19 (No. 6), 717–728. doi:10.3319/tao.2008.19.6.717(pt)

Coltelli, M., Cavallaro, D., Firetto Carlino, M., Cocchi, L., Muccini, F., D'Alessandro, A., et al. (2016). The marine Activities Performed within the TOMO-ETNA experiment. *Ann. Geophys.* 59 (4), S0428. doi:10.4401/ag-7081

Cuffaro, M., Billi, A., Bigi, S., Bosman, A., Caruso, C. G., Conti, A., et al. (2019). The Bortoluzzi Mud Volcano (Ionian Sea, Italy) and its Potential for Tracking the Seismic Cycle of Active Faults. *Solid Earth* 10, 741–763. doi:10.5194/se-10-741-2019

Dahm, T., Thorwart, M., Flueh, E. R., Braun, T., Herber, R., Favali, P., et al. (2002). Ocean Bottom Seismometers Deployed in Tyrrhenian Sea. *Eos Trans. AGU* 83 (29), 309–315. doi:10.1029/2002eo000221

De Caro, M., Monna, S., Frugoni, F., Beranzoli, L., and Favali, P. (2014). Seafloor Seismic Noise at Central Eastern Mediterranean Sites. *Seismological Res. Lett.* 85, 1019–1033. doi:10.1785/0220130203

Devoti, R., Riguzzi, F., Cuffaro, M., and Doglioni, C. (2008). New GPS Constraints on the Kinematics of the Apennines Subduction. *Earth Planet. Sci. Lett.* 273, 163–174. doi:10.1016/j.epsl.2008.06.031

Díaz, J., Gallart, J., and Gaspà, O. (2007). Atypical Seismic Signals at the Galicia Margin, North Atlantic Ocean, Related to the Resonance of Subsurface Fluid-Filled Cracks. *Tectonophysics* 433, 1–13. doi:10.1016/j.tecto.2007.01.004

Doglioni, C. (1991). A Proposal for the Kinematic Modelling of W-Dipping Subductions - Possible Applications to the Tyrrhenian-Apennines System. *Terra Nova* 3 (4), 423–434. doi:10.1111/j.1365-3121.1991.tb00172.x

Doglioni, C., Innocenti, F., and Mariotti, G. (2001). Why Mt Etna? *Terra Nova* 13 (1), 25–31. doi:10.1046/j.1365-3121.2001.00301.x

Doglioni, C., Merlini, S., and Cantarella, G. (1999). Foredeep Geometries at the Front of the Apennines in the Ionian Sea (central Mediterranean). *Earth Planet. Sci. Lett.* 168 (3-4), 243–254. doi:10.1016/s0012-821x(99)00059-x

Embriaco, D., Marinaro, G., Frugoni, F., Monna, S., Etiope, G., Gasperini, L., et al. (2014). Monitoring of Gas and Seismic Energy Release by Multiparametric Benthic Observatory along the North Anatolian Fault in the Sea of Marmara (NW Turkey). *Geophys. J. Int.* 196, 850–866. doi:10.1093/gji/ggt436

Favali, P., Beranzoli, L., and De Santis, A. (2015). *Seafloor Observatories: A New Vision of the Earth from the Abyss*. Berlin, Germany; Heidelberg, Germany: Springer-Verlag. doi:10.1007/978-3-642-11374-1

Favali, P., and Beranzoli, L. (2006). Seafloor Observatory Science: a Review. *Ann. Geophys.* 49 (2/3), 515–567. doi:10.4401/ag-3125

Franek, P., Plaza-Faverola, A., Mienert, J., Buenz, S., Ferré, B., and Hubbard, A. (2017). Microseismicity Linked to Gas Migration and Leakage on the Western Svalbard Shelf. *Geochem. Geophys. Geosyst.* 18, 4623–4645. doi:10.1002/2017GC007107

Gallais, F., Graindorge, D., Gutscher, M.-A., and Klaeschen, D. (2013). Propagation of a Lithospheric Tear Fault (STEP) through the Western Boundary of the Calabrian Accretionary Wedge Offshore Eastern Sicily (Southern Italy). *Tectonophysics* 602, 141–152. doi:10.1016/j.tecto.2012.12.026

Gallais, F., Gutscher, M.-A., Klaeschen, D., and Graindorge, D. (2012). Two-stage Growth of the Calabrian Accretionary Wedge in the Ionian Sea (Central Mediterranean): Constraints from Depth-migrated Multichannel Seismic Data. *Mar. Geol.* 326-328, 28–45. doi:10.1016/j.margeo.2012.08.006

Gutscher, M.-A., Dominguez, S., de Lepinay, B. M., Pinheiro, L., Gallais, F., Babonneau, N., et al. (2016). Tectonic Expression of an Active Slab Tear from High-Resolution Seismic and Bathymetric Data Offshore Sicily (Ionian Sea). *Tectonics* 35, 39–54. doi:10.1002/2015tc003898

Hino, R., Kanazawa, T., and Hasegawa, A. (1996). Interplate Seismic Activity Near the Northern Japan Trench Deduced from Ocean Bottom and Land-Based Seismic Observations. *Phys. Earth Planet. Interiors* 93, 37–52. doi:10.1016/0031-9201(95)03087-5

Hsiao, N.-C., Lin, T.-W., Hsu, S.-K., Kuo, K.-W., Shin, T.-C., and Leu, P.-L. (2014). Improvement of Earthquake Locations with the Marine Cable Hosted Observatory (MACHO) Offshore NE Taiwan. *Mar. Geophys. Res.* 35, 327–336. doi:10.1007/s11001-013-9207-3

Husen, S., Kissling, E., and Flueh, E. R. (2000). Local Earthquake Tomography of Shallow Subduction in north Chile: A Combined Onshore and Offshore Study. *J. Geophys. Res.* 105 (B12), 28183–28198. doi:10.1029/2000jb900229

INGV Seismological Data Centre (2006). *Rete Sismica Nazionale (RSN)*. Italy: Istituto Nazionale di Geofisica e Vulcanologia (INGV). doi:10.13127/SD/X0FXNH7QFY

ISIDe Working Group (2007). *Italian Seismological Instrumental and Parametric Database (ISIDe)*. Rome: Istituto Nazionale di Geofisica e Vulcanologia (INGV). doi:10.13127/ISIDE

Lawton, J., Frohlich, C., Pulpan, H., and Latham, G. V. (1982). Earthquake Activity at the Kodiak continental Shelf, Alaska, Determined by Land and Ocean Bottom Seismograph Networks. *Bull. Seismol. Soc. Am.* 72, 207–220. doi:10.1785/bssa0720010207

Loher, M., Ceramicola, S., Wintersteller, P., Meinecke, G., Sahling, H., and Bohrmann, G. (2018). Mud Volcanism in a Canyon: Morphodynamic Evolution of the Active Venere Mud Volcano and its Interplay with Squillace Canyon, Central Mediterranean. *Geochem. Geophys. Geosyst.* 19, 356–378. doi:10.1002/2017GC007166

Maesano, F. E., Tiberti, M. M., and Basili, R. (2017). The Calabrian Arc: Three-Dimensional Modelling of the Subduction Interface. *Sci. Rep.* 7, 8887. doi:10.1038/s41598-017-09074-8

Mariotti, G., and Doglioni, C. (2000). The Dip of the Foreland Monocline in the Alps and Apennines. *Earth Planet. Sci. Lett.* 181, 191–202. doi:10.1016/s0012-821x(00)00192-8

Matsuzawa, T., Hirose, H., Shibazaki, B., and Obara, K. (2010). Modeling Short- and Long-term Slow Slip Events in the Seismic Cycles of Large Subduction Earthquakes. *J. Geophys. Res. Solid Earth* 115 (B12), B12301. doi:10.1029/2010jb007566

McNamara, D. E., and Buland, R. P. (2004). Ambient Noise Levels in the continental United States. *Bull. Seismol. Soc. Am.* 94 (4), 517–527. doi:10.1785/012003001

McNamara, D. E., Hutt, C. R., Gee, L. S., Benz, H. M., and Buland, R. P. (2009). A Method to Establish Seismic Noise Baselines for Automated Station Assessment. *Seismological Res. Lett.* 80 (4), 628–637. doi:10.1785/gssrl.80.4.628

Minelli, L., and Faccenna, C. (2010). Evolution of the Calabrian Accretionary Wedge (central Mediterranean). *Tectonics* 29, TC4004. doi:10.1029/2009tc002562

Monna, S., Sgroi, T., and Dahm, T. (2013). New Insights on Volcanic and Tectonic Structures of the Southern Tyrrhenian (Italy) from marine and Land Seismic Data. *Geochem. Geophys. Geosyst.* 14 (9), 3703–3719. doi:10.1002/ggge.20227

Montuori, C., Cimini, G. B., and Favali, P. (2007). Teleseismic Tomography of the Southern Tyrrhenian Subduction Zone: New Results from Seafloor and Land Recordings. *J. Geophys. Res.* 112 (B3), B03311. doi:10.1029/2005JB004114

Palano, M., Schiavone, D., Loddo, M., Neri, M., Presti, D., Quarto, R., et al. (2015). Active Upper Crust Deformation Pattern along the Southern Edge of the Tyrrhenian Subduction Zone (NE Sicily): Insights from a Multidisciplinary Approach. *Tectonophysics* 657, 205–218. doi:10.1016/j.tecto.2015.07.005

Peccerillo, A. (2005). *Plio-quaternary Volcanism in Italy*, 365. New York: Springer-Verlag Berlin Heidelberg.

Peterson, J. (1993). Observation and Modeling of Seismic Background Noise. US Geological Survey Open File Report. Albuquerque, NM, USA: US Geological Survey, 93–322.

Polonia, A., Nelson, C. H., Romano, S., Vaiani, S. C., Colizza, E., Gasparotto, G., et al. (2017b). A Depositional Model for Seismo-Turbidites in Confined Basins Based on Ionian Sea Deposits. *Mar. Geol.* 384, 177–198. doi:10.1016/j.margeo.2016.05.010

Polonia, A., Torelli, L., Artoni, A., Carlini, M., Faccenna, C., Ferranti, L., et al. (2016). The Ionian and Alfeo-Etna Fault Zones: New Segments of an Evolving Plate Boundary in the central Mediterranean Sea? *Tectonophysics* 675, 69–90. doi:10.1016/j.tecto.2016.03.016

Polonia, A., Torelli, L., Gasperini, L., Cocchi, L., Muccini, F., Bonatti, E., et al. (2017a). Lower Plate Serpentinite Diapirism in the Calabrian Arc Subduction Complex. *Nat. Commun.* 8, 2172. doi:10.1038/s41467-017-02273-x

Polonia, A., Torelli, L., Gasperini, L., and Mussoni, P. (2012). Active Faults and Historical Earthquakes in the Messina Straits Area (Ionian Sea). *Nat. Hazards Earth Syst. Sci.* 12, 2311–2328. doi:10.5194/nhess-12-2311-2012

Polonia, A., Torelli, L., Mussoni, P., Gasperini, L., Artoni, A., and Klaeschen, D. (2011). The Calabrian Arc Subduction Complex in the Ionian Sea: Regional Architecture, Active Deformation, and Seismic hazard. *Tectonics* 30, TC5018. doi:10.1029/2010TC002821

Presti, D. (2019). Seismicity Supports the Theory of Incipient Rifting in the Western Ionian Sea, central Mediterranean. *Ann. Geopysics* 62 (2), SE225. doi:10.4401/ag-8360

Sánchez-Reyes, H., Essing, D., Beaucé, E., and Poli, P. (2021). The Imbricated Foreshock and Aftershock Activities of the Balsorano (Italy) 4.4 normal Fault Earthquake and Implications for Earthquake Initiation. *Seismol. Res. Lett.* 92, 1926–1936. doi:10.1785/0220200253

Sgroi, T., Beranzoli, L., Di Grazia, G., Ursino, A., and Favali, P. (2007). New Observations of Local Seismicity by the SN-1 Seafloor Observatory in the Ionian Sea, Off-Shore Eastern Sicily (Italy). *Geophys. J. Int.* 169 (2), 490–501. doi:10.1111/j.1365-246X.2007.03348.x

Sgroi, T., Braun, T., Dahm, T., and Frugoni, F. (2006). An Improved Seismicity Picture of the Southern Tyrrhenian Area by the Use of OBS and Land-Based Network: the TYDE experiment. *Ann. Geophys.* 49 (2-3), 801–817. doi:10.4401/ag-3130

Sgroi, T., De Nardis, R., and Lavecchia, G. (2012). Crustal Structure and Seismotectonics of central Sicily (Southern Italy): New Constraints from Instrumental Seismicity. *Geophys. J. Int.* 189 (3), 1237–1252. doi:10.1111/j.1365-246X.2012.05392.x

Sgroi, T., Di Grazia, G., and Favali, P. (2019). Volcanic Tremor of Mt. Etna (Italy) Recorded by NEMO-SN1 Seafloor Observatory: a New Perspective on Volcanic Eruptions Monitoring. *Geosciences* 9 (3), 115. doi:10.3390/geosciences9030115

Sgroi, T., Monna, S., Embriaco, D., Giovanetti, G., Marinaro, G., and Favali, P. (2014). Geohazards in the Western Ionian Sea: Insights from Non-earthquake Signals Recorded by the NEMO-SN1 Seafloor Observatory. *Oceanography* 27 (2), 154–166. doi:10.5670/oceanog.2014.51

Sgroi, T., Montuori, C., Agrusta, R., and Favali, P. (2009). Low-frequency Seismic Signals Recorded by OBS at Stromboli Volcano (Southern Tyrrhenian Sea). *Geophys. Res. Lett.* 36 (4), L04305. doi:10.1029/2008GL036477

Sgroi, T., Polonia, A., Barberi, G., Billi, A., and Gasperini, L. (2021). New Seismological Data from the Calabrian Arc Reveal Arc-Orthogonal Extension across the Subduction Zone. *Sci. Rep.* 11, 473. doi:10.1038/s41598-020-79719-8

Sohn, R. A., Hildebrand, J. A., Webb, S. C., and Fox, C. G. (1995). Hydrothermal microseismicity at the Megaplume site on the southern Juan de Fuca Ridge. *Bull. Seismol. Soc. America* 85, 775–778.

Sultan, N., Riboulot, V., Ker, S., Marsset, B., Géli, L., Tary, J. B., et al. (2011). Dynamics of Fault-Fluid-Hydrate System Around a Shale-Cored Anticline in deepwater Nigeria. *J. Geophys. Res.* 116, B12110. doi:10.1029/2011JB008218

Tary, J. B., Géli, L., Guennou, C., Henry, P., Sultan, N., Çağatay, N., et al. (2012). Microevents Produced by Gas Migration and Expulsion at the Seabed: A Study Based on Sea Bottom Recordings from the Sea of Marmara. *Geophys. J. Int.* 190, 993–1007. doi:10.1111/j.1365-246X.2012.05533.x

Totaro, C., Presti, D., Billi, A., Gervasi, A., Orecchio, B., Guerra, I., et al. (2013). The Ongoing Seismic Sequence at the Pollino Mountains, Italy. *Seismol. Res. Lett.* 84, 955–962. doi:10.1785/0220120194

Webb, S. C. (2002). "19 Seismic Noise on Land and on the Sea Floor," in *International Handbook of Earthquake and Engineering Seismology*. Editors W. H. K Lee, H. Kanamori, P. C. Jennings, and C. Kisslinger (Amsterdam, Netherlands: Academic Press), 81, 305–318. doi:10.1016/s0074-6142(02)80222-4

Webb, S. C. (1998). Broadband Seismology and Noise under the Ocean. *Rev. Geophys.* 36, 105–142. doi:10.1029/97rg02287

Webb, S. C., and Crawford, W. C. (2010). Shallow-water Broadband OBS Seismology. *Bull. Seismol. Soc. America* 100 (4), 1770–1778. doi:10.1785/0120090203

Zhang, H., Thurber, C., and Bedrosian, P. (2009). Joint Inversion for Vp, vs, and Vp/Vs at SAFOD, Parkfield, California. *Geochem. Geophys. Geosyst.* 10 (11), Q11002. doi:10.1029/2009GC002709

Conflict of Interest: The authors declare that the research was conducted in the absence of any commercial or financial relationships that could be construed as a potential conflict of interest.

Publisher's Note: All claims expressed in this article are solely those of the authors and do not necessarily represent those of their affiliated organizations, or those of the publisher, the editors and the reviewers. Any product that may be evaluated in this article, or claim that may be made by its manufacturer, is not guaranteed or endorsed by the publisher.